Measurement report: Intra/interannual variability and source apportionment of VOCs during 2018–2020 in Zhengzhou, Central China

Shijie Yu [a,b], Shenbo Wang[b,c], Ruixin Xu [b,c], Dong Zhang [a,b], Meng Zhang [e], Fangcheng Su[b,c], Xuan Lu[a,b], Xiao Li[b,c], Ruiqin Zhang [b,c]*, Lingling Wang [d]*

a. College of Chemistry, Zhengzhou University, Zhengzhou 450001, China

b. Institute of Environmental Sciences, Zhengzhou University, Zhengzhou 450001, China

c. School of Ecology and Environment, Zhengzhou University, Zhengzhou 450001, China

d. Environmental Monitoring Center of Henan Province，Zhengzhou 450000

e. Pingdingshan Ecological Environment Monitoring Center of Henan Province, Pingdingshan 467000, China

*Correspondence author. Research Institute of Environmental Science, College of Environment and Ecology, Zhengzhou University High-tech Development Zone, Zhengzhou, Henan, PR China, 450001

E-mail address: rqzhang@zzu.edu.cn

Abstract:

Ambient volatile organic compounds (VOCs) were measured continuously from January 2018 to December 2020 at an urban site in Zhengzhou (China) to investigate their characteristics, sources, atmospheric oxidation capacity (AOC), and chemical reactivity. During the sampling period, the total concentration of observed VOCs was 94.3 ± 53.1 $\mu g/m^3$ ppbv and alkanes were the major VOC species, accounting for 58% of the total. During the sampling period, the interannual variation of VOCs gradually reduced from 113.2 ± 65.2 $\mu g/m^3$ in 2018, 90.7 ± 52.5 $\mu g/m^3$ in 2019, and 79.1 ± 41.7 $\mu g/m^3$ in 2020. Ethane and propane were the top two most abundant species during the three-year observation period. Results showed that the total AOC, dominated by OH radical reactions, was 7.4×10^7 molecules cm^{-3} s^{-1}. Total OH reactivity was 45.3 s^{-1} and it was mainly contributed by NOx. The AOC and •OH reactivity both exhibited well-defined seasonal and interannual patterns. Therefore, control strategies should focus on the key species given their interannual and seasonal variations. Meanwhile, diagnostic ratios of VOC species indicated that VOCs in Zhengzhou were greatly affected by vehicle emissions and liquid petroleum gas/natural gas (LPG/NG). Positive matrix factorization analysis identified six sources: industrial sources, solvent use, vehicle emissions, LPG/NG, fuel burning, and biogenic sources. Vehicle emissions and industrial sources made the largest contributions to VOC emission in each of the three years. The proportion of the contributions of vehicle emissions and LPG/NG increased with each passing year. However, the proportion of industrial and solvent sources presented a decreasing trend, which reflects the remarkable effect of control policies. The effect of VOCs on O_3 formation suggests that vehicle emissions and solvent use remain key sources. Therefore, it is necessary to formulate effective strategies for reducing ground-level O_3, and those sources mentioned above should be strictly controlled by the regulatory authorities.

1. Introduction

In recent years, regional atmospheric pollution events have occurred frequently

around the world, with many areas suffering severe haze episodes in autumn and winter, and O_3 pollution in summer (Uttamang et al., 2020; Li et al., 2019; Sadeghi et al., 2021; Yan et al., 2018; Yadav et al., 2019; Zhang et al., 2018). Volatile organic compounds (VOCs) are important precursors of secondary pollutants such as O_3 and secondary organic aerosols, and the study of VOCs is a primary focus among the scientific community and relevant governing bodies (Liu et al., 2019a; Song. et al., 2019c; Xu et al., 2017).

VOCs encompass a large variety of species, and the chemical reactivity of each species varies greatly. Thus, elucidation of VOC characteristics and active substance identification represent research priorities. In many regions, alkanes represent the dominant VOC species, while studies which do not report OVOCs usually identify aromatics and alkenes as better contributors of ozone formation potential (OFP) (Li et al., 2019b; Yan et al., 2017). Following a study in Wuhan (China), Yang et al. (2019) suggested that alkanes were the dominant group, accounting for 42% of the total VOC concentration, and that C_2-C_3 hydrocarbons were the dominant active substance. Huang and Hsieh (2019) studied the maximum incremental reactivity (MIR) and propylene-equivalent (PE) concentration, reporting that toluene was the largest potential contributor to the OFP and that industrial emissions contributed nearly 60% to the OFP. Given the complex composition of VOCs in the atmosphere, it is difficult to determine the sources of VOCs. To apportion the source contributions of VOCs, it is common practice to use receptor models that include positive matrix factorization (PMF), chemical mass balance, and principal component analysis. In China, traffic emissions are often the main source of VOCs, particularly in major metropolitan areas (Li et al., 2019; Liu et al., 2019; Song, et al., 2019b). Moreover, industrial processes and solvent use have remarkable influence on VOC emissions (Hui et al., 2019; Mo et al., 2017). Biogenic sources also cannot be ignored owing to their high reactivity, which can contribute 5%–20% of VOC emissions (Wu et al., 2016). In addition to the study of VOC characteristics and source apportionment, analysis of atmospheric oxidation characteristics is another area of hot topic. Variations in the atmospheric oxidation capacity (AOC) not only affect the O_3 level in summer but also greatly

77　impact the generation of secondary particles throughout the entire year (Prinn, 2003).

78　However, most previous related studies in China focused on metropolitan areas such

79　as the Beijing–Tianjin–Hebei region (Gu et al., 2019b), Pearl River Delta region

80　(Zhang et al., 2015), and Yangtze River Delta region (Xu et al., 2017; Zheng et al.,

81　2020), while less research has been conducted in heavily polluted areas of the central

82　plains. Moreover, previous studies frequently used short-term monitoring data that

83　cannot fully reflect the comprehensive VOC pollution characteristics within a region.

84　Therefore, it is an urgent requirement that large-scale investigations be conducted on

85　the central plains of China.

86　　　As the political and cultural center of Henan Province, Zhengzhou had more than

87　10 million permanent residents and 4.0 million private vehicles in 2019 (Gu et al.,

88　2019a). This area is often confronted with severe haze episodes and photochemical

89　pollution due to emission of huge amounts of air pollutants (Li et al., 2020b).

90　Consequently, much research has been conducted on air pollution in Zhengzhou, but

91　many of the earlier studies focused only on particulate matter (Jiang et al., 2018;

92　Wang et al., 2019). Few studies have addressed VOCs in Zhengzhou, especially in

93　relation to longer sampling periods and seasonal measurements. Following adjustment

94　of control policies and optimization of the energy structure, recent mitigation

95　measures might have affected the characteristics and sources of VOCs. Therefore, it is

96　necessary to identify local VOC pollution characteristics on the basis of a long time

97　series of monitoring data, which could provide a reference for formulation of local air

98　pollution control measures.

99　　　To deepen the understanding of VOC pollution characteristics, chemical

100　reactivity, and source contribution, VOC data were measured in Zhengzhou using

101　online instruments from 2018–2020. The aims of this research were as follows: (1)

102　analyze the characteristics of VOC variation in Zhengzhou, including diurnal,

103　seasonal, and annual changes; (2) quantify the contribution of sources among

104　intra/interannual variations and identify the locations of VOC sources; (3)

105　parameterize the AOC and speciate OH reactivity; and (4) assess O_3 formation by

106　MIR and PE analysis.

2. Methodology

2.1 Study site and measurements

The observation period of this study was from January 2018 to December 2020. The VOC samples were collected at an urban site (34°45′N, 113°41′E) by the Department of Environmental Protection of Henan Province. The surrounding environment represents a typical urban environment in Zhengzhou, comprising commercial and residential districts with traffic sources (Fig. 1).

The VOC species were monitored continuously using an auto-GC system with a 1-h time resolution (AMA Instruments GmbH, Germany). Specific information regarding this system is described in Zou et al. (2015). The 57 VOC species (comprising 29 alkanes, 10 alkenes, 1 alkyne, and 17 aromatics) were calibrated using the VOC Standards of the U.S. EPA PAMS mixture (Spectra Gases, USA) before monitoring. During the observation period, zero and span gas checks (PAMS calibration gases) were conducted monthly using the 5-point method, together with adjustment of the retention time. Data quality control of this instrument is detailed in our previous study (Ren et al., 2020). Overall, the correlation coefficient varied from 0.990–0.999, and the detection limits were in the range of 0.02–0.12 ppbv, as shown in Table S1.

Meteorological data comprising atmospheric temperature (T), relative humidity, ultraviolet (UV) radiation, precipitation (Pr), planetary boundary layer height, wind speed (WS), and wind direction (WD) were obtained from the surface meteorological station of the Henan monitoring center. Datasets of trace gases such as the hourly concentrations of NO, NO_2, CO, O_3, SO_2, and fine particles ($PM_{2.5}$) were obtained from the ambient air quality observation station of Yanchang, which is located approximately 2 km from the VOC monitoring station.

2.2 Positive matrix factorization (PMF) model

In this study, analysis of the source of the VOCs was performed using the EPA

134 PMF 5.0 model, which is a receptor model used widely for source apportionment

135 (Gao et al., 2018; Yadav et al., 2019). Detailed information regarding this method is

136 available in the user manual (Norris et al., 2014) and other related literature (Song et

137 al., 2019a, 2019b). Two input files are required for PMF: the concentration values and

138 the uncertainty values of the individual VOC species. The uncertainty is calculated

139 using Eq. (1) when the species concentration value is higher than its method detection

140 limit (MDL), or using Eq. (2) when the concentration is less than or equal to the

141 MDL:

$$\mathrm{Unc} = \sqrt{(\mathrm{EF} \times c)^2 + (0.5 \times \mathrm{MDL})^2}, \qquad (1)$$

$$\mathrm{Unc} = \frac{5}{6} \times \mathrm{MDL}, \qquad (2)$$

144 where c is the concentration of the individual VOC species, and EF is the error

145 fraction, which was set to 10% of the VOC concentration (Yuan et al., 2012).

146 Owing to the complexity of the chemical reactions, not all of the VOC species

147 were used in the PMF analysis. Based on previous work, this study adopted the

148 following principles for selection of the VOC species. (1) Species with more than

149 25% of data missing or below the MDLs were rejected, which follows the

150 methodology of previous studies (Zhou et al., 2019). (2) Species with short

151 atmospheric lifetimes were excluded because they rapidly react away in the

152 atmosphere. (3) Species that represent source tracers of emission sources were

153 retained (e.g., in the case of isoprene). Eventually, 26 VOC species were selected for

154 source apportionment analysis. VOC species were grouped into strong, weak and bad

155 according to their signal/noise ratio (S/N), and there were 22 and 4 species grouped

156 into strong and weak, respectively. It should be noted that the volumetric

157 concentration (ppbv) of the individual VOC species was converted to mass

158 concentration ($\mu g\ m^{-3}$) before being input into the PMF model.

159 Choosing the optimal number of factors in the model is important. The number

160 of factors depends on Q (ture)/Q (robust) and Q/Qexpected (Qexp). In theory, Q

161 (ture)/Q (robust) < 1.5 and a value close to 1 is considered reasonable (Ulbrich et al.,

162 2009), and the rate of change of Q/Qexp should be stable and the ratio should be close

163   to 1 (Baudic et al., 2016; Hui et al., 2019). In this study, the numbers of factors used

164   for the PMF analysis were tested from three to eight, and the optimum six-factor

165   solution with Q/Qexp = 0.94, (Q (ture)/Q (robust) = 1.0) was selected. Additionally,

166   Fpeak values from −1 to 1 with 0.1 intervals were used in the model, and Fpeak = -0.2

167   was established as the best solution (as shown in Fig. S1).

2.3 Relative reactivity of VOCs

169   To better understand the role of VOCs in the formation of tropospheric O_3, the

170   OFP and the PE concentration were investigated to analyze the chemical reactivity of

171   the VOC species (Carter, 1994; Atkinson and Arey, 2003), and the detailed operation

172   is described in the supplementary materials (Text S1).

2.4 Atmospheric oxidation capacity (AOC) and speciated oxidant reactivity

174   The AOC is defined as the sum of the respective oxidation rates of the primary

175   pollutants (e.g., CO, CH_4, and VOCs) by the oxidants (e.g., OH, NO_3, and O_3), and it

176   can be calculated using Eq. (3) (Elshorbany et al., 2009; Xue et al., 2016):

$$AOC = \sum_i k_{Yi}[X][Y_i], \qquad (3)$$

178   where $[X]$ and $[Y_i]$ are the number concentrations of molecule oxidant X and Y_i,

179   respectively, and k_{Yi} is the bimolecular rate constant of molecule Y_i with oxidant X

180   (Zhu et al., 2020). In this study, the reduced substances only included 57 PAMS

181   (provided by Spectra Gases Inc., USA) and CO. The oxidants only included •OH,

182   NO_3, and O_3 radicals. The concentration OH and NO_3 radicals was estimated from

183   parameterization methods via Eqs. (4) and (5) (Carter, 1994; Warneke, 2004):

$$[OH] = a \times (J_{O^1D})^\alpha \times (J_{NO_2})^\beta \times \frac{b \times [NO_2] + 1}{c \times [NO_2]^2 + d \times [NO_2] + 1}, (4)$$

185   where J_{O1D} and J_{NO2} are the measured photolysis frequency (s^{-1}) of O_3 and NO_2,

186   respectively. The values of a, b, c, α, and β are 4.1×10^9, 140, 0.41, 1.7, 0.83, and 0.19,

187   respectively (Yang et al., 2019).

188   NO_3 concentration in the atmosphere is based on the steady-state assumption

189   (Liebmann et al., 2018):

$$[NO_3] = \frac{k_{NO_2} \times [NO_2] \times [O_3]}{J_{NO_3} + J_{NO+NO_3} \times [NO] + \sum_i k_{NO_3+VOC_i} \times [VOC]_i}, \qquad (5)$$

where J_{NO3} is the measured photolysis frequency (s^{-1}) of NO_3. The rate coefficients for NO_2-O_3 (k_{NO2+O3}) and NO-NO_3 (k_{NO+NO3}) were obtained from Atkinson et al. (2004). Detailed descriptions of the calculation processes of OH and NO_3 are available in Yang et al. (2021).

Additionally, OH reactivity is another indicator of atmospheric oxidation. It is the inverse of the OH lifetime, and it can be defined as the product of the rate coefficients and the concentrations of the reactants with OH. Thus, OH reactivity can be calculated using Eq. (6) (Mao et al., 2010):

$$OH\ reactivity = \sum k_{OH+VOC_i} \times [VOC_i] + k_{OH+CO} \times [CO] + k_{OH+NO} \times [NO] +$$

$$k_{OH+NO_2} \times [NO_2] \qquad\qquad + k_{OH+SO_2} \times [SO_2] + k_{OH+O_3} \times [O_3] + k_{OH+other} \times$$

$$[other], \qquad (6)$$

where $[Xi]$ is the concentration of the species (e.g., CO, NOx, SO_2, and VOCs), and the rate coefficient k_{OH} (unit: cm^3 molecule1 s^{-1}) represents the corresponding reaction rate coefficient.

2.5 Conditional probability function (CPF) analysis

The conditional probability function (CPF) was developed to identify potential source contributions using the PMF source contribution solution, coupled with WD (Guo et al., 2011; Hsu et al., 2018; Wu et al., 2016). The CPF is defined as follows:

$$CPF = \frac{m_{\triangle\theta}}{n_{\triangle\theta}}, \qquad (7)$$

where $m_{\triangle\theta}$ is the number of appearances from wind sector $\triangle\theta$ (each sector is 22.5°) that exceed the concentration threshold (75th percentile of each source contribution), and $n_{\triangle\theta}$ is the total number of occurrences in the same wind sector. Weak winds (WS < 1.5 m s^{-1}) were excluded from the calculation because of the difficulty in defining WD (Zheng et al., 2018).

3. Results and discussion

3.1 Characteristics of VOCs in Zhengzhou

3.1.1 Concentrations and compositions of VOCs

The average ambient VOC concentrations and chemical species measured in Zhengzhou during the study period are shown in Table S2. And Table S3 presented the comparison of VOCs between this study and other studies. The annual average concentration of VOCs was 94.3±53.1 μg/m^3 (38.2±15.6 ppbv), i.e., close to the concentration reported in Langfang (33.4 ppbv) (Song et al., 2019a) and Nanjing (34.4 ppbv) (Shao, et al. 2016), lower than that found in Chengdu (41.8 ppbv) (Song et al. 2018), Guangzhou (42.7 ppbv) (Zou et al., 2015), and higher than that reported in Tianjin (28.7 ppbv) (Liu et al. 2016). Among the observed species, alkanes were the major component of the VOCs with mean concentration of 54.7±37.9 μg/m^3, accounting for 58% of the total, followed by aromatics (25%), alkenes (13%) and alkynes (3%). Many previous related studies also reported that alkanes represent the dominant group (Fu et al., 2020; Gu et al., 2020), similar to the situation found in Zhengzhou. For the record, OVOCs were not simultaneously measured in this study due to the limitations on available instrumentation. Thus, those investigations apply only to studies which failed to measure OVOCs.

To clarify the characteristics of VOC emission sources, the concentrations of the 20 most abundant species, accounting for 83% of the compound classes monitored in the present study, are listed in Table 1. During the sampling period (2018–2020), the most important VOC species in Zhengzhou were ethane (11.7±6.8 μg/m^3), propane (8.2±4.9μg/m^3), toluene (6.5±4.5μg/m^3), i-pentane (6.1±10.4 μg/m^3), n-butane(5.8±4.1μg/m^3) and ethene (5.6±5.3μg/m^3). Generally, C_2-C_5 species are closely related to vehicular emissions, coal burning, and liquid petroleum gas (LPG) (Hui et al., 2021; Zhang, et al. 2020). Among the most abundant 20 VOC species, half were alkanes, accounting for 79% of the total alkanes measured. The C_2-C_3 alkanes mainly originate from LPG, while C_4-C_5 alkanes are considered tracers of vehicle

243 emissions (Fan et al., 2021). The most abundant alkene species were ethylene,

244 propene, isoprene, and propene, representing 72% of the total alkanes. The C_2-C_3

245 alkenes are mainly derived from vehicle emissions and LPG (Zhang et al., 2015),

246 whereas isoprene is a typical biogenic tracer (Maji et al., 2020). And isoprene

247 emissions have also been reported from biomass burning e.g. from smouldering rice

248 straw fires (Kumar et al., 2021). In the 20 most abundant VOC species, there were 6

249 aromatics: toluene, m p-xylene, benzene, ethylbenzene, o-xylene and

250 p-diethylbenzene. These aromatics are the most frequently observed aromatic

251 compounds in urban areas, originating from vehicle emissions, industrial processes,

252 solvent use, and combustion sources (Hui et al., 2019).

253 **3.1.2 Interannual variation of VOCs**

254   The interannual average concentrations and contributions of VOCs during

255 2018–2020 are presented in Table S2. The interannual variation of the VOCs declined

256 gradually as follows: 113.2±65.2 μg/m^3 in 2018, 90.7±52.5 μg/m^3 in 2019, and

257 79.1±41.7 μg/m^3 in 2020. It should be mentioned is the differences in these yearly

258 averages are statistically significant considering the large standard deviations

259 indicated. The trend of decrease of VOCs could be attributed to increasingly stringent

260 policies regarding emission reduction and the influence of the COVID-19 lockdown

261 on air quality in 2020 (Wang et al., 2021a).

262   The concentrations of the 20 most abundant species are listed in Table 1. Ethane

263 and propane were the top two most abundant species in each of the three years,

264 indicating that LPG and vehicular emissions had substantial impact on the area

265 surrounding the sampling site (Yadav et al., 2019). The C_4-C_5 alkanes and some

266 aromatics represent the main tracers of motor vehicle emissions (Fan et al., 2021).

267 However, the quantities of those species were diminished in 2020, which might

268 represent a consequence of the COVID-19 epidemic. As a tracer of coal burning,

269 acetylene decreased gradually from 4.8±4.9 μg/m^3 in 2018 to 0.9±1 μg/m^3 in 2020.

3.1.3 Seasonal variations

As plotted in Fig. S2 and listed in Table S4, the monthly mean mixing ratios of the VOCs and compounds were investigated. The VOCs showed clear seasonal dependence with highest concentration in winter (116.5 $\mu g/m^3$) followed by spring (86.4 $\mu g/m^3$), autumn (86.1 $\mu g/m^3$), and summer (74.2 $\mu g/m^3$). Meanwhile, the seasonal variation of the group of alkanes, alkenes, alkynes, and aromatics was similar to that of the VOCs. Additionally, the monthly mean mixing ratios of the dominant and tracer species are plotted in Fig. 2. The results show that almost all VOCs had clear seasonal dependence, with highest concentrations in winter and lowest concentrations in summer. However, the mixing ratio of isoprene was highest (2.46 $\mu g/m^3$) in July and lowest (0.33 $\mu g/m^3$) in December. As a tracer of biogenic sources, isoprene showed positive correlation with T ($R^2 = 0.61$, $p < 0.01$). In addition to biogenic emissions, the seasonal variation of VOCs was mainly influenced by changes of anthropogenic sources. As a northern city of China, Zhengzhou emits substantial quantities of pollutants during the heating season in winter (Wang et al., 2019). The higher concentrations of VOCs and tracers (such as acetylene and aromatics) in winter might be derived from coal combustion (Zhang et al., 2020).

Seasonal variations in VOC concentrations are associated with several factors such as photochemical activities and meteorological conditions. In summer, VOCs are consumed under the condition of high T, strong UV radiation, and high concentration of OH radicals (Huang et al., 2019). In winter, the high level of VOCs can often be attributed to a lower boundary layer and calm weather conditions (Hui et al., 2019). Additionally, the transport of pollutants from the Beijing–Tianjin–Hebei region cannot be ignored because of the north wind that prevails in Zhengzhou in winter. The seasonal variation of VOCs in several cities was investigated and the variation trend of VOC concentrations in most studies were found similar to that observed in Zhengzhou (Liu et al., 2019; Yadav et al., 2019).

3.1.4 Diurnal variations

The diurnal variations in VOCs, trace gases (NO_2 and O_3), and meteorological parameters (T, relative humidity, WS, and UV) are shown in Fig. S3. The VOCs present negative correlation with O_3 ($R^2 = -0.82$, $p < 0.01$), whereas the diurnal variation of VOCs shows moderate consistency with the variation of NO_2 ($R^2 = 0.62$, $p < 0.01$). The high values of VOCs generally appeared in the morning with low O_3 concentrations. The peak in the morning was attributed to vehicle emission (Li et al., 2019b). Additionally, local meteorological and atmospheric processes also play important roles in the diurnal variation of VOCs in ambient air. In the early morning, the concentrations of VOCs remained high owing to stable atmospheric conditions and a shallow boundary layer height (Hui et al., 2020). The concentration of VOCs declined to the lowest value at 15:00 China Standard Time (CST), when O_3 reached a maximum level with the production and consumption rates of O_3 in equilibrium. In the afternoon, higher T and increased UV radiation intensity led to consumption of VOCs. Moreover, higher WS also accelerated the diffusion of VOCs. Subsequently, VOC concentrations gradually accumulated with the arrival of the late traffic peak, and remained at a high level throughout the night. It should be noted that VOC concentrations at night were generally higher than those during the day. Previous studies have suggested that VOCs can be oxidized by O, OH radicals, and NO_3 radicals (Atkinson and Arey, 2003). During the daytime, reactions with OH radicals and O_3 are the most important chemical reactions for VOCs, whereas the reactions with NO_3 radicals and O_3 are the main sedimentation reactions at night. Concentrations of VOCs were generally higher at night because the chemical activity of OH radicals is much higher than that of NO_3 radicals (Carter, 2010).

The mean diurnal variations of high-concentration and tracer VOCs were investigated, as shown in Fig. 3. As tracers of motor vehicle emissions (Zheng et al., 2018), i-pentane and n-pentane showed remarkable peaks at 08:00 CST that are considered to reflect vehicle emissions. Furthermore, benzene, toluene, ethylbenzene, xylene, and the C_2-C_4 alkanes also presented similar diurnal variation characteristics

that are considered to represent the substantial effect of motor vehicles. However, the mixing ratio of isoprene showed higher values in the afternoon and had a trend similar to that of T. The elevated values of isoprene in the afternoon indicated substantial emissions from biogenic sources.

3.2 Diagnostic ratios

Some VOC species are commonly used as indicators of emission sources. To characterize the seasonal differences in the contributions of the various sources, this study adopted the benzene/toluene (B/T) ratio and the i-pentane/n-pentane ratio as the preferred metrics.

The B/T ratio can be used to distinguish potential sources such as traffic emissions, coal+biomass combustion, and solvent use. The diagnostic ratios varied according to the emission sources (i.e., below 0.20 for solvent use, 0.5 for traffic sources, 1.5–2.2 for coal combustion, and 2.5 for biomass burning) (Huang et al., 2019; Li et al., 2019a). As shown in Fig. S4, the highest value of the B/T ratio was 0.55 in winter, suggesting that traffic emissions affected the ambient atmosphere. The ratios of 0.31, 0.27, and 0.31 in spring, summer, and autumn, respectively, indicate that aromatics were more likely derived from the mixed sources of solvent use and vehicle emissions during these seasons. As a transportation hub, Zhengzhou has a large number of motor vehicles (Gu et al., 2019a). Therefore, regional controls on motor vehicle use should be strengthened.

The i-pentane/n-pentane ratio was also investigated. Generally, i-pentane and n-pentane have similar reaction rates with OH radicals, and the ratio of this pair of species is indicative of different sources. The i-pentane/n-pentane ratio associated with coal combustion, vehicle emissions, and fuel evaporation is generally 0.56–0.80, ~ 2.2, and 3.8, respectively (Huang et al., 2019; Li et al., 2019a). The highest i-pentane/n-pentane ratio was found in summer (2.79), indicating strong impact from traffic sources. The ratio was 1.88 in spring and 1.96 in autumn, suggesting that most VOCs originated from the mixed sources of vehicle emissions and coal combustion.

354   Notably, the average ratio in winter (1.55) was lower than that in the other three

355   seasons, indicating stronger contribution from coal burning in the heating season.

356   **3.3 Source identification**

357   In this study, six sources were identified using the PMF model: industrial sources,

358   solvent use, vehicle emissions, LPG/natural gas (NG), fuel burning, and biogenic

359   sources. The source profiles of the VOCs during the sampling period are presented in

360   Fig. 4.

361   **3.3.1 Factor 1: industrial sources**

362   Factor 1 was characterized by high loadings on ethylene (60.6%), ethane (31.6%),

363   propylene (25.8%), and propane (24.0%). Ethene and propylene are the first and

364   second most abundant industrially produced organic compounds worldwide,

365   respectively (Eckert et al., 2014). Additionally, this factor was also dominated by

366   aromatics such as styrene (76.0%), toluene (34.3%), and ethylbenzene (28.1%), which

367   are typical tracers of industrial sources. Meanwhile, this source had correlation with

368   gas tracers of NO_2, SO_2, and CO (R^2 = 0.47, 0.36, and 0.49, respectively). CO and

369   $NO2$ are mainly gases from combustions sources strongly influenced by urban

370   activities such as traffic and domestic heating. Instead, SO_2 is generally mainly due to

371   industrial sources or combustion of heavy oils and coals. Therefore, source 1 was

372   assigned to industrial sources.

373   The CPF plots indicated the dominant source directions as northeast and

374   southeast, which correspond to industrial estates (as shown in Fig. 5). Moreover, the

375   highest VOC concentration from industrial sources was observed at 10:00 CST,

376   probably attributable to increased industrial activities during daytime.

377   **3.3.2 Factor 2: solvent use**

378   Factor 2 was characterized by high levels of n-hexane (60.4%), n-octane (26.3%),

379   methyl   cyclohexane   (20.4%),   o-xylene   (79.6%),   m/p-xylene   (61.7%),   p-

14

380 diethylbenzene (84.0%), o-xylene (79.0%), m-ethyl toluene (57.8%), o-ethyl toluene

381 (29.2%), ethylbenzene (51.1%), and toluene (20.8%). These compounds are major

382 components emitted through the use of various solvents or industrial processes (Zhou

383 et al. 2019, Wang et al. 2021). However, there were almost no tracers of ethane,

384 ethene, acetylene, and benzene related to combustion sources, and this source

385 appeared to exhibit poor correlation with gas tracers ($R^2 < 0.10$). Therefore, source 2

386 was identified as solvent use.

387   The CPF plots of this factor suggested southeast was the dominant source

388 direction, possibly reflecting the presence of the large manufacturers of automobiles

389 in the southeastern urban area.

390 **3.3.3 Factor 3: vehicle emissions**

391   Factor 3 was identified by high percentages of C2-C6 alkanes (i.e., ethane

392 (37.8%), propane (46.9%), iso-butane (40.9%), n-butane (38.5%), n-pentane (26.0%),

393 and i-pentane (31.6%)), C2-C4 alkanes (i.e., ethylene (31.4%), propylene (38.4%),

394 and 1-butene (67.4%)), and C6-C8 aromatics (i.e., benzene (21.4%), toluene (30.7%),

395 and m/p-xylene (25.6%)). These components are considered typical products of

396 incomplete combustion processes (Baudic et al., 2016; Gaimoz et al., 2011; Liu et al.,

397 2008a; Song et al., 2018). It is reported that i-pentane usually originates from gasoline

398 evaporation (Mo et al., 2017), and that 2-methylpentane and 3-methylpentane are

399 tracers of the emissions of gasoline-powered vehicles (Tsai et al., 2003; Liu et al.,

400 2008; Song et al., 2018). The T/B ratio was 2.0 in this profile, which further confirms

401 the effect of vehicular emissions (Yao et al., 2021). Moreover, the source correlated

402 significantly with CO and NO_2 ($p < 0.01$), but not with SO_2 ($p > 0.05$); therefore,

403 source 3 was identified as vehicle emissions.

404   Factor 3 showed larger CPF values when the wind came from the north, possibly

405 because the site is adjacent to Jinshui Road, which is the main road in Zhengzhou.

406 The diurnal pattern of the traffic source was characterized by two peaks: one in the

407 morning and the other in the evening, consistent with the relative strength of local

408   traffic flow.

409   3.3.4 Factor 4: LPG/NG

410   Factor 4 was dominated by strong presence of ethane (16.3%), propane (14.6%),

411   iso-butane (38.9%), n-butane (44.4%), n-pentane (60.3%), and i-pentane (66.2%),

412   which can also be released via fuel evaporation (gasoline and LPG/NG) (Zhang et al.,

413   2019). Pentanes are the most abundant VOC species associated with gasoline

414   evaporation (Liu et al., 2008; Zhang et al., 2013; Shen et al., 2018), and butanes are

415   reported as tracers of LPG (McCarthy et al., 2013). In particular, the aromatics of this

416   source were very low. Similar to factor 3, the source did not correlate with SO_2 (p >

417   0.05), but had positive correlation with both CO and NO_2 (p < 0.01); therefore, this

418   source was considered as LPG/NG.

419   The dependence of factor 4 on WD was not as significant as for other sources. It

420   is related to compact residential areas with greater human activity. There are

421   residential areas around the monitoring site, and LPG/NG leakage might have

422   occurred in the process of daily life.

423   3.3.5 Factor 5: fuel burning

424   Factor 5 was distinguished by substantial amounts of acetylene (72%), which is a

425   marker of combustion sources (Hui et al., 2021). Additionally, the source was also

426   characterized by considerable amounts of benzene and C_2-C_3 hydrocarbons, which are

427   representative species of incomplete combustion processes (Zheng et al., 2021).

428   Meanwhile, the independent tracers (i.e., NO_2, SO_2, and CO) exhibited correlation

429   with this factor (R^2 > 0.3, p < 0.01); therefore, source 5 was considered to be fuel

430   burning.

431   Factor 5 displayed high CPF values when the wind was from east. This is

432   possibly related to the heating companies located within 1.0 km to the east of the site.

433   The diurnal variation of this factor was characterized by apparent increase at night,

434   which could be related to the accumulation of pollutants associated with nighttime

435 heating.

3.3.6 Factor 6: biogenic sources

437 Factor 6 exhibited a significantly high composition of isoprene, which is mainly
438 produced by vegetation through photosynthesis (Song et al., 2019a). Accordingly,
439 source 6 was labeled as biogenic sources.

440 The CPF plots indicated that this factor mainly originated from the west with
441 conditional probability values of approximately 0.44. It is mainly affected by
442 Zijinshan Park, which is located ~1 km to the west of the monitoring site.
443 Additionally, the diurnal pattern of the biogenic sources showed obvious T
444 dependence, with the highest concentration at midday that could be associated with
445 photosynthetic activity.

3.3.7 Comparison between the composite source profiles and the PMF factors

447 As shown in Fig. S5, the source profiles derived from the PMF analysis were
448 compared with their sources attributed from the source profiles. The data of the source
449 profiles were derived from a local tunnel experiment and a review of the most recent
450 literature. The source profiles for solvent use correlated most strongly between the
451 two methods (R = 0.84). A study by Jin et al. (2022) identified that low-carbon
452 alkanes (e.g., ethane, propane, and isopentane), alkenes (e.g., ethylene, propene, and
453 1-butene), and aromatics (e.g., benzene, toluene, and m/p-xylene) were the main
454 groups in the tunnel study, and that vehicle emissions agreed well between this factor
455 and the source profiles (R = 0.59). Different profiles of combustion sources were
456 investigated, and the correlation between the results of NG combustion and the PMF
457 factor was strongest (R = 0.57). The above results are to be expected because
458 Zhengzhou has gradually phased out coal-fired boilers and replaced them with gas
459 boilers in recent years. As for industrial sources, the correlation between the two
460 methods was 0.43. The C_2-C_3 hydrocarbons accounted for a high proportion in factor
461 1, whereas the content of aromatics was lower. Industrial production of nonmetallic

mineral products in Zhengzhou is reasonably well developed, which leads to large emissions of ethane and propane. The main contributing source of aromatic hydrocarbons is rubber and plastics. However, the scale of the enterprises involved in their production is far lower than that in the Pearl River Delta; consequently, the emission of aromatic hydrocarbons is lower in Zhengzhou.

3.4 VOC source contributions

3.4.1 Interannual variation

The concentration contributions of each VOC source during 2018–2020 are shown in Fig. 6. In 2018, vehicular emissions were the largest contributor to VOC mixing ratios (32%), followed by industrial sources (21%), solvent use (19%), and LPG/NG (15%). The contribution of fuel burning and biogenic sources accounted for 9% and 4% of the total VOC concentration, respectively. As for 2019, vehicle emissions made the largest contribution (38%) to atmospheric VOCs. The second most significant source was industrial sources, accounting for 18% of the total. The contribution of solvent use, LPG/NG, fuel burning, and biogenic sources to atmospheric VOCs was 17%, 15%, 11%, and 2%, respectively, in 2019. Vehicular emissions, LPG/NG, industrial sources, solvent use, fuel burning, and biogenic sources accounted for 39%, 18%, 17%, 15%, 9%, and 3%, respectively, in 2020

In summary, vehicle emissions and industrial sources made the largest contributions in all three years. Moreover, the proportions of the contributions of vehicle emissions and LPG/NG have increased with each passing year. As a transportation hub city, the number of motor vehicles in Zhengzhou has maintained a rate of growth of 0.4 million annually during the past five years, and the total number of vehicles exceeded 4.5 million in 2020 (Gu et al., 2019a). Thus, vehicle emissions represent an important source of ambient VOCs in Zhengzhou. Both LPG and NG are used widely in residential life, industrial production, and motor vehicles. In terms of the actual situation of the monitoring site, residential emissions might represent the main source of LPG/NG. With adjustment of the energy structure, most industrial

490   enterprises and taxis in Zhengzhou now use NG as energy or fuel. It should be noted

491   that the proportion of the contributions from industrial and solvent sources has

492   presented an annual downward trend. In recent years, Zhengzhou has implemented

493   special actions designed to reduce VOC emissions, focusing on the control of

494   industrial and scattered small-scale pollution enterprises. According to the results

495   obtained using the PMF model, it is speculated that the effect of such policy control

496   has been remarkable.

497   **3.4.2 Seasonal variation**

498   Owing to different meteorological conditions and emission strengths, the source

499   contributions vary seasonally. As shown in Fig. 7, the seasonal variation of biogenic

500   emissions was substantial, with the highest contribution in summer (7%) and the

501   lowest contribution in winter (<1%). This might reflect both T and UV intensity.

502   Conversely, the contributions from fuel burning were larger in winter and lower in

503   summer. Fuel burning accounted for a larger proportion of emissions in winter (17%)

504   than in summer (3%). Meanwhile, industrial emissions contributed a high percentage

505   of VOCs in spring (22%), whereas the contributions in the other three seasons were

506   comparable. Additionally, motor vehicle emissions showed no obvious seasonal

507   characteristics, and the contribution to atmospheric VOCs in each of the four seasons

508   exceeded 30% of the total, indicating that motor vehicles have considerable impact on

509   the air quality of Zhengzhou.

510   **3.4.3 Comparison with other studies**

511   3.4.3.1 Comparison with emission inventory (EI) studies

512   This study compared the annual average relative contributions of different

513   sources with results from published emission inventory (EI) studies. In the

514   anthropogenic VOC emission inventories established by Lu et al. (2020), VOC

515   sources were classified into eight categories: stationary combustion, on-road mobile

516   sources, non-road mobile sources, industrial processes, solvent use sources, fuel oil

517   storage and transportation, biomass burning, and others. Vehicle emissions

518   represented the most abundant source of anthropogenic VOCs in both the EI and the

519   PMF analysis, accounting for 29.7% and 36.3% of the total, respectively. The

520   differences observed between the EI and PMF results were primarily because most of

521   the vehicles considered were in urban areas. The contributions of industrial sources

522   and of solvent use sources represented the second and third largest, respectively, in

523   both the EI and the PMF results. However, the overall contribution of those two

524   sources obtained from the PMF results was lower than that derived from the EI

525   analysis. The relative contribution of combustion sources resolved from the PMF

526   analysis was higher than that obtained from the EI results, accounting for 9.5% and

527   4.3%, respectively. Such large differences occurred primarily because of uncertainties

528   in the activity data obtained from statistical information. Residential energy

529   consumption and emissions were poorly recorded in comparison with other sources

530   (Chen et al., 2016; Tao et al., 2018), leading to higher uncertainties in the related

531   estimations of such emissions. Thus, it is necessary to estimate the emissions of

532   residential fossil fuel combustion through scientific approaches.

533   3.4.3.2 Comparison with other PMF studies

534   The source contributions determined in this research were also compared with

535   the results from other studies. It can be seen from Table 2 that the source

536   apportionment of VOCs in this study was broadly within the values reported for other

537   Chinese cities (Huang et al., 2019; Hui et al., 2018; Li et al., 2020c; Mo et al., 2017;

538   Yan et al., 2017). It was found that traffic emissions represent the main source of

539   VOCs in Zhengzhou and the other five cities, indicating that vehicle emissions have

540   considerable impact on the concentration of VOCs in the urban atmosphere. It should

541   be noted that the contribution of each source determined in this study was very similar

542   to that reported for Wuhan (Hui et al., 2018). Given that Zhengzhou and Wuhan are

543   both important transportation hub cities in central China, this result is in line with

544   expectation.

3.5 AOC

The AOC during the sampling periods was quantified, as shown in Fig. 8. The calculated averaged value of total AOC was 7.4×10^7 molecules cm^{-3} s^{-1}, comparable with values reported for a suburban site between Beijing and Tianjin (Yang et al., 2020b), but substantially higher than observed in Shanghai (Zhu et al., 2020), Hong Kong (Xue et al., 2016), Chile (Elshorbany et al., 2009), and Berlin (Geyer et al., 2001). Among the AOC categories, OH exhibited the highest average concentration (7.0×10^7 molecules cm^{-3} s^{-1}), accounting for 95% of the total AOC, followed by O_3 (3.4×10^6 molecules cm^{-3} s^{-1}) and NO_3 (1.1×10^5 molecules cm^{-3} s^{-1}), which contributed 4% of the total AOC. Thus, OH is the main contributor of atmospheric oxidation in Zhengzhou, similar to the results reported for other regions by other studies (Yang et al., 2021; Zhu et al., 2020).

During 2018–2020, the total AOC presented a decreasing trend annually (as shown in Fig. 8), with mean values of 8.0, 6.4, and 6.2×10^7 molecules cm^{-3} s^{-1}, respectively. As expected, OH was the predominant oxidant in each of the three years, accounting for 95%, 95%, and 97% of the total AOC, respectively. The primary pollutants (e.g., CO, CH_4, and VOCs) decreased significantly in 2020 owing to large reductions in economic activity and the associated emissions during the COVID-19 lockdown. However, the average OH concentration was highest in 2020 (4.8×10^7 molecules cm^{-3}), far higher than that in either of the two previous years. Thus, the level of atmospheric oxidation needs additional attention. It should be noted that oxidation of the atmosphere did not decrease or even increase significantly during the epidemic, which has been reported by many previous studies (Wang et al., 2021b).

As shown in Fig. S7, the mean AOC values showed pronounced seasonal variation. The highest total AOC value was detected in summer (7.5×10^7 molecules cm^{-3} s^{-1}), followed by winter (6.4×10^7 molecules cm^{-3} s^{-1}), spring (5.8×10^7 molecules cm^{-3} s^{-1}), and autumn (5.7×10^7 molecules cm^{-3} s^{-1}). The concentration of OH in summer was significantly higher than that in the other seasons, which can be ascribed to the relatively favorable meteorological conditions. Meanwhile, high

574 concentrations of isoprene were observed in summer, and its high reaction rate

575 coefficients with oxidants (e.g., OH, NO_3, and O_3) revealed a highly oxidative

576 environment during the summer campaign in Zhengzhou. This seasonal pattern of the

577 AOC is similar to that found in other studies conducted at the national level, and in

578 urban and suburban environments (Yang et al., 2021; Li et al., 2020a).

579 **3.6 Atmospheric environmental implications**

580 **3.6.1 OH reactivity of measured species**

581 The calculated OH reactivity was categorized into SO_2, NO_2, NO, O_3, CO, and

582 VOCs, as shown in Fig. 9. During the sampling period, the average value of total OH

583 reactivity was 45.3 s^{-1}. Generally, the OH reactivity assessed in this study was much

584 higher than that determined in Shanghai (Tan et al., 2019; Zhu et al., 2020),

585 Chongqing (Tan et al., 2019), and New York (Ren et al., 2006), but comparable with

586 or lower than that reported in Xianghe (Yang et al.,2020a) and Backgarden (Lou et al.,

587 2010). In Zhengzhou, NO_2 made the largest contribution to total OH reactivity (54%),

588 followed by VOCs (17%), NO (16%), CO (11%), SO_2 (3%), and O_3 (1%). Similar

589 results were reported by previous studies conducted in other regions (Yang et al.,

590 2021). It should be noted that this study calculated only the OH reactivity of the

591 measured species, i.e., the impact of unmeasured species, such as secondary products

592 (oxygenated VOCs and nitrates produced by photochemical reactions) and

593 monoterpenes, were not considered. Previous studies have shown that both undetected

594 primary emissions and unmeasured secondary products could contribute to missing

595 reactivity (Yang et al., 2016). Therefore, the value of OH reactivity determined in this

596 study was underestimated to a certain extent.

597 OVOCs play an important role to influence the AOC via OH-initiated

598 degradation. A previous review suggested that missing OH reactivity has often been

599 observed, and the difference compared the measured and calculated was attributed to

600 a lack of measurement data for OVOCs (Yang et al., 2016). Steiner et al. (2008) found

601 that OVOCs accounted for 30–50% of the modelled urban VOC reactivity by using

the regional Community Multiscale Air Quality model (CMAQ). In another urban study, OVOCs were found to contribute between 11–24% during summertime in Houston (Mao et al., 2010b). In the CareBeijing-2006 and PRIDE-PRD campaigns, Lou et al., (2010) and lu et al., (2013) reported the significant contributions of OVOCs to OH reactivity based on model simulations. Since OVOCs were not simultaneously measured in four Chinese megacities, the OVOC contributions were simulated with a box model. And OVOCs explained between 20% and 23% to the total OH reactivity (Tan et al., 2019). In summary, OVOCs behaved as a major contributor to the total OH reactivity.

Table S5 shown the OH reactivity towards the total VOCs and the comparison with other studies. The OH reactivity of the total VOCs was 6.7 s^{-1}, i.e., much lower than that reported for Heshan (13.6 s^{-1}) (Yang et al., 2017) and Beijing (8.3 s^{-1}) (Yang et al., 2021), but close to that found in Guangzhou (6.4 s^{-1}) and Chongqing (6.8 s^{-1}) (Tan et al., 2019) and higher than that determined in Shanghai (3.2 s^{-1}) (Tan et al., 2019). The detailed contributions of each VOC group to total OH reactivity are presented in Tables S6 and S7. The contribution of alkenes to OH reactivity was predominant, accounting for 5.2 s^{-1} of the total OH reactivity of VOCs. During the sampling period, isoprene made the largest contribution to the OH reactivity of the total VOCs, followed by ethene, m/p-xylene, propene, styrene, cis-2-butene, trans-2-butene, toluene, i-pentane, and trans-2-pentene, which collectively accounted for 70% of the OH reactivity of the total VOCs.

As shown in Fig. 9, OH reactivity showed substantial interannual and seasonal variations. The statistical results exhibit a decreasing trend of OH reactivity during 2018–2020 in Zhengzhou with mean values of 50.2, 46.9, and 36.9 s^{-1}, respectively. This trend might reflect the implementation of emission reduction measures such as traffic-related measures and the "Coal to Gas" project. The OH reactivity in 2020 was 21% lower than that in the previous year, which is closely related to the emission reduction associated with the COVID-19 epidemic. Seasonally, the mean value of OH reactivity decreased in the following order: winter (74.5 s^{-1}) > autumn (48.6 s^{-1}) > spring (43.1 s^{-1}) > summer (31.8 s^{-1}). The notable differences might be attributable to

632   higher loadings of reactive trace gases, especially NOx and CO. As a northern city,

633   coal combustion in Zhengzhou during the heating season produces higher

634   concentrations of NOx and CO, leading to higher OH reactivity. Therefore, we should

635   continually strengthen policies to control trace gases, especially in autumn and winter.

636   The OH reactivity of the total VOCs was similar with the higher value in winter (7.3

637   s^{-1}) and the lower value in autumn (5.3 s^{-1}). However, the concentrations of the key

638   species were markedly different among the four seasons. Ethylene and propylene had

639   highest OH reactivity in winter, which is speculated to be related to the emission of

640   combustion sources. Additionally, isoprene made the largest contribution to the total

641   OH reactivity in both summer and spring, reflecting the substantial effect of biogenic

642   sources. Overall, the research on specific OH reactivity clearly elucidated the seasonal

643   and annual variations of the major reactants. Therefore, control strategies based on

644   OH reactivity should focus on the key species.

645   **3.6.2 Effect of VOCs on O_3 formation**

646   Because VOCs are important precursors of O_3 formation in the ground-level

647   atmosphere, it is necessary to adequately estimate the contribution of each VOC

648   species to O_3 formation. The concentration contributions of the four VOCs categories

649   expressed on different scales from 2018–2020 are shown in Fig. S8. The result

650   suggests that aromatics made the largest contribution to the MIR concentration,

651   accounting for a combined ratio of 81%. Meanwhile, alkenes were the largest

652   contributors to the PE concentration (87%). Although the concentrations of aromatics

653   and alkenes are relatively low, these two VOC groups play an important role in O_3

654   formation, which is a result supported by many previous studies (Hui et al., 2021; Li

655   et al., 2020b). It should be noted that the effect of VOCs on O3 formation were

656   calculated from the sum of measured species, and does not involve species that were

657   not measured, such as OVOCs. Therefore, we provided a lower limit of the effect of

658   VOCs on O_3 formation in this study.

659   Among the top 10 reactive species contributing to the PE and MIR weighted

concentrations (as shown in Fig. 10), 8 compounds were the same, differing only in their rank order.The top 10 VOCs obtained from the PE and MIR methods represent 67% and 74% of VOCs, respectively. Considering kinetic activity, isoprene ranked first (8.8 ppbC) with the PE method, accounting for approximately 20% of the total PE concentration, and m,p-xylene, styrene, ethene, and toluene ranked second to fifth, explaining 16%, 10%, 7%, and 5% of the total OFP, respectively. In comparison, ethene, m/p-xylene, toluene, propane, and isoprene had the highest MIR concentrations, which accounted for approximately 23%, 21%, 12%, 7%, and 7%, respectively. The results of this study highlight the contributions of isoprene, ethene, m/p-xylene, and toluene to O_3 formation, and these species are derived primarily from vehicle emissions and industrial coatings (Xiong and Du, 2020).

On the basis of the results of source apportionment, the source contributions to OFP and PE were calculated (shown in Fig. S9). Vehicle emissions made the greatest contribution to O_3 formation (OFP: 23%; PE: 29%), followed by solvent use (OFP: 25%; PE: 24%). However, the contribution of biogenic emissions accounting for 22% of the total PE cannot be ignored. Because of the discrepancy between the MIR weighted and PE weighted concentrations, the contribution of this source to OFP was relatively low, accounting for only 6%. The PE concentration method considers only the kinetic reactivity of VOC species and ignores mechanism reactivity, whereas the MIR method considers the impact of the VOC/NOx ratio on O_3 formation.

4. Conclusions

In this study, hourly observational data of 57 VOC species were collected during 2018–2020 at an urban site in Zhengzhou (China). The results showed that the average total VOC mixing ratio was 94.3±53.1 μg/m3 (38.2±15.6 ppbv), and that the VOC concentrations were dominated by alkanes in each of the three years. During the sampling period, the interannual variation of VOCs gradually reduced as follows: 113.2±65.2 μg/m3 in 2018, 90.7±52.5 μg/m3 in 2019, and 79.1±41.7 μg/m3 in 2020. The VOCs showed clear seasonal dependence with the highest value in winter (116.5

μg/m^3) and lowest value in summer (74.2 μg/m^3). The PMF method was used to identify six sources: vehicle emissions (36%), solvent use (17%), LPG/NG (16%), industrial sources (18%), fuel burning (10%), and biogenic sources (3%). The proportion of both vehicle emissions and LPG/NG has increased with each passing year. However, the proportion of industrial and solvent sources presented a decreasing trend. In addition to substantial interannual variation, the VOC sources also showed marked seasonal differences. The contribution of vehicle emissions to the atmosphere in each of the four seasons was >30%. Atmospheric VOCs are affected substantially by fuel burning (17%) in winter; however, the influence of biogenic sources cannot be ignored (7%) in summer.

This study also focused on the atmospheric environmental implications of VOCs, including the AOC, OH reactivity, and OFP. During the sampling periods, the campaign-averaged value of the total AOC was 7.4×10^7 molecules cm^{-3} s^{-1}, and OH exhibited the highest average concentration, accounting for 95% of the total AOC. The average value of the total OH reactivity was 45.3 s^{-1}, and NO$_2$ made the largest contribution to the total OH reactivity (54%), followed in descending order by VOCs (17%), NO (16%), CO (11%), SO$_2$ (3%), and O$_3$ (1%). Investigation of the effects of VOCs on O$_3$ formation revealed that despite the relatively low concentrations of aromatics and alkenes, they played important roles in O$_3$ formation. Ethene, m/p-xylene, and toluene contributed substantially to O$_3$ formation in Zhengzhou. The source apportionment results indicate that vehicle emissions and solvent use remain the key sources of the VOCs that contribute to O$_3$ formation.

Overall, investigation of the concentrations, source apportionment, and atmospheric environmental implications clearly elucidated the differences in the major reactants observed in different seasons and years. Therefore, control strategies should consider seasonal and interannual variations when focusing on the key species and sources. The results of this study could support local governments in developing strategies to control VOCs during O$_3$ pollution events.

Data availability

718

719   The data set is available to the community and can be accessed by request from

720   Ruiqin Zhang (rqzhang@zzu.edu.cn).

721

722

Author contribution

723

724   YSJ and ZRQ planned and organized the study, and were deeply involved in

725   writing the manuscript. WSB, XRX and ZD performed the atmospheric measurements

726   and data analysis and wrote the manuscript. ZM and WLL assisted heavily with the

727   atmospheric measurements and data analysis. SFC and LX and LX conducted the

728   model development and data analysis.

729   Other coauthors provided useful insights in data analysis and contributed to the

730   writing of the manuscript.

731   We thank James Buxton, MSc, from Liwen Bianji (Edanz)

732   (www.liwenbianji.cn/), for editing the English text of a draft of this manuscript.

733

Acknowledgments

References

Atkinson, R., Arey, J., 2003. Atmospheric degradation of volatile organic compounds. Chem. Rev. 103, 4605-4638.

Atkinson, R., Baulch, D., Cox, R., Crowley, J., Hampson, R., Hynes, R., Jenkin, M., Rossi, M., Troe, J., 2004. Evaluated kinetic and photochemical data for atmospheric chemistry: volume I - gas phase reactions of Ox, HOx, NOx and SOx species. Atmos. Chem. Phys. 4, 1461-1738.

Baudic, A., Gros, V., Sauvage, S., Locoge, N., Sanchez, O., Sarda-Estève, R., Kalogridis, C., Petit, J.E., Bonnaire, N., Baisnée, D., Favez, O., 2016. Seasonal variability and source apportionment of volatile organic compounds (VOCs) in the Paris megacity (France). Atmos. Chem. Phys. 16, 11961–11989.

Carter, W., 1994. Development of ozone reactivity scales for volatile organic compounds. J. Air Waste Manag. Assoc. 44, 881-899.

Carter, W., 2010. Development of the SAPRC-07 chemical mechanism. Atmos. Environ. 44, 5324-5335.

Elshorbany, Y., Kurtenbach, R., Wiesen, P., Lissi, E., Rubio, M., Villena, G., Gramsch, E., Rickard, A., Pilling, M., Kleffmann, J., 2009. Oxidation capacity of the city air of Santiago, Chile. Atmos. Chem. Phys. 9, 2257-2273.

Fan, M., Zhang, Y., Lin, Y., Li, L., Xie, F., Hu, J., Mozaffar, A., Cao, F., 2021. Source apportionments of atmospheric volatile organic compounds in Nanjing, China during high ozone pollution season. Chemosphere. 263, 128025.

Fu, S., Guo, M., Luo, J., Han, D., Chen, X., Jia, H., Jin, X., Liao, H., Wang, X., Fan, L., Cheng, J., 2020. Improving VOCs control strategies based on source characteristics and chemical reactivity in a typical coastal city of South China through measurement and emission inventory. Sci. Total Environ. 744, 140825.

Gao, J., Zhang, J., Li, H., Li, L., Xu, L., Zhang, Y., Wang, Z., Wang, X., Zhang, W., Chen, Y., Cheng, X., Zhang, H., Peng, L., Chai, F., Wei, Y., 2018. Comparative study of volatile organic compounds in ambient air using observed mixing ratios

767   and initial mixing ratios taking chemical loss into account - A case study in a

768   typical urban area in Beijing. Sci. Total Environ. 628-629, 791-804.

769 Garzn, J., Huertas, J., Magaa, M., Huertas, M., Crdenas, B., Watanabe, T., Maeda, T.,

770   Wakamatsu, S., Blanco, S., 2015. Volatile organic compounds in the atmosphere

771   of Mexico city. Atmos. Environ. 119, 415-429.

772 Geyer, A., Alicke, B., Konrad, S., Schmitz, T., Stutz, J., Platt, U., 2001. Chemistry and

773   oxidation capacity of the nitrate radical in the continental boundary layer near

774   Berlin. J. Geophys. Res.-Atmos. 106, 8013-8025.

775 Gu, X., Yin, S., Lu, X., Zhang, H., Wang, L., Bai, L., Wang, C., Zhang, R., Yuan, M.,

776   2019a. Recent development of a refined multiple air pollutant emission inventory

777   of vehicles in the central plains of China. J. Environ. Sci (in China). 84, 80-96.

778 Gu, Y., Li, Q., Wei, D., Gao, L., Tan, L., Su, G., Liu, G., Liu, W., Li, C., Wang, Q.,

779   2019b. Emission characteristics of 99 NMVOCs in different seasonal days and

780   the relationship with air quality parameters in Beijing, China. Ecotoxicol.

781   Environ. Saf. 169, 797-806.

782 Gu, Y., Liu, B., Li, Y., Zhang, Y., Bi, X., Wu, J., Song, C., Dai, Q., Han, Y., Ren, G.,

783   Feng, Y., 2020. Multi-scale volatile organic compound (VOC) source

784   apportionment in Tianjin, China, using a receptor model coupled with 1-hr

785   resolution data. Environ. Pollut. 265, 115023.

786 Guo, H., Cheng, H., Ling, Z., Louie, P., Ayoko, G., 2011. Which emission sources are

787   responsible for the volatile organic compounds in the atmosphere of Pearl River

788   Delta. J. Hazard. Mater. 188, 116-124.

789 Hsu, C., Chiang, H., Shie, R., Ku, C., Lin, T., Chen, M., Chen, N., Chen, Y., 2018.

790   Ambient VOCs in residential areas near a large-scale petrochemical complex:

791   Spatiotemporal variation, source apportionment and health risk. Environ. Pollut.

792   240, 95-104.

793 Huang, X., 2020. Evaluating the effectiveness of multiple emission control measures

794   on reducing volatile organic compounds in ambient air based on observational

795   data: A case study during the 2010 Guangzhou Asian Games. Sci. Total Environ.

796   723, 138171.

797   Huang, Y., Hsieh, C., 2019. Ambient volatile organic compound presence in the

798   highly urbanized city: source apportionment and emission position. Atmos.

799   Environ. 206, 45-59.

800   Hui, L., Liu, X., Tan, Q., Feng, M., An, J., Qu, Y., Zhang, Y., Jiang, M., 2018.

801   Characteristics, source apportionment and contribution of VOCs to ozone

802   formation in Wuhan, Central China. Atmos. Environ. 192, 55-71.

803   Hui, L., Liu, X., Tan, Q., Feng, M., An, J., Qu, Y., Zhang, Y., Cheng, N., 2019. VOC

804   characteristics, sources and contributions to SOA formation during haze events

805   in Wuhan, Central China. Sci. Total Environ. 650, 2624-2639.

806   Hui, L., Liu, X., Tan, Q., Feng, M., An, J., Qu, Y., Zhang, Y., Deng, Y., Zhai, R.,

807   Wang,Z., 2020. VOC characteristics, chemical reactivity and sources in urban

808   Wuhan, central China. Atmos. Environ. 224,117340.

809   Hui, L., Ma, T., Gao, Z., Gao, J., Wang, Z., Xue, L., Liu, H., Liu, J., 2021.

810   Characteristics and sources of volatile organic compounds during high ozone

811   episodes: A case study at a site in the eastern Guanzhong Plain, China.

812   Chemosphere. 265,129072.

813   Jiang, N., Duan, S., Yu, X., Zhang, R., Wang, K., 2018. Comparative major

814   components and health risks of toxic elements and polycyclic aromatic

815   hydrocarbons of $PM_{2.5}$ in winter and summer in Zhengzhou: Based on three-year

816   data. Atmos. Res. 213, 173-184.

817   Li, B., Ho, S., Gong, S., Ni, J., Li, H., Han, L., Yang, Y., Qi, Y., Zhao, D., 2019a.

818   Characterization of VOCs and their related atmospheric processes in a central

819   Chinese city during severe ozone pollution periods. Atmos. Chem. Phys. 19,

820   617-638.

821   Li, K., Li, J., Tong, S., Wang, W., Huang, R.-J., Ge, M., 2019b. Characteristics of

822   wintertime VOCs in suburban and urban Beijing: concentrations, emission ratios,

823   and festival effects. Atmos. Chem. Phys. 19, 8021-8036.

824   Li, Q., Badia, A., Wang, T., Sarwar, G., Fu, X., Zhang, L., Zhang, Q., Fung, J., Cuevas,
825   C., Wang, S., Zhou, B., Saiz-Lopez, A., 2020a. Potential effect of halogens on
826   atmospheric oxidation and air quality in China. J. Geophys. Res-atmos. 125,
827   e2019JD032058.

828   Li, Y., Yin, S., Yu, S., Yuan, M., Dong, Z., Zhang, D., Yang, L., Zhang, R., 2020b.
829   Characteristics, source apportionment and health risks of ambient VOCs during
830   high ozone period at an urban site in central plain, China. Chemosphere. 25,
831   126283.

832   Li, Q., Su, G., Li, C., Liu, P., Zhao, X., Zhang, C., Sun, X., Mu, Y., Wu, M., Wang, Q.,
833   Sun, B., 2020c. An investigation into the role of VOCs in SOA and ozone
834   production in Beijing, China. Sci. Total. Environ. 720, 137536.

835   Liebmann, J., Muller, J., Kubistin, D., Claude, A., Holla, R., Plass-Dülmer, C.,
836   Lelieveld, J., Crowley, J., 2018. Direct measurements of NO_3 reactivity in and
837   above the boundary layer of a mountaintop site: identification of reactive trace
838   gases and comparison with OH reactivity. Atmos. Chem. Phys. 18, 12045-12059.

839   Liu, B., Liang, D., Yang, J., Dai, Q., Bi, X., Feng, Y., Yuan, J., Xiao, Z., Zhang, Y., Xu,
840   H., 2016. Characterization and source apportionment of volatile organic
841   compounds based on 1-year of observational data in Tianjin, China. Environ.
842   Pollut. 218, 757-769.

843   Liu, Y., Song, M., Liu, X., Zhang, Y., Hui, L., Kong, L., Zhang, Y., Zhang, C., Qu, Y.,
844   An, J., Ma, D., Tan, Q., Feng, M., 2019a. Characterization and sources of volatile
845   organic compounds (VOCs) and their related changes during ozone pollution
846   days in 2016 in Beijing, China. Environ. Pollut. 257, 113599.

847   Liu, Y., Wang, H., Jing, S., Gao, Y., Peng, Y., Lou, S., Cheng, T., Tao, S., Li, L., Li, Y.,
848   Huang, D., Wang, Q., An, J., 2019b. Characteristics and sources of volatile
849   organic compounds (VOCs) in Shanghai during summer: Implications of
850   regional transport. Atmos. Environ. 215, 116902.

851   Lou, S., Holland, F., Rohrer, F., Lu, K., Bohn, B., Brauers, T., Chang, C., Fuchs, H.,

Häseler, R., Kita, K., Kondo, Y., Li, X., Shao, M., Zeng, L., Wahner, A., Zhang, Y., Wang, W., and Hofzumahaus, A., 2010. Atmospheric OH reactivities in the Pearl River Delta – China in summer 2006: measurement and model results, Atmos. Chem. Phys. 10, 11243-11260.

Maji, S., Beig, G., Yadav, R., 2020. Winter VOCs and OVOCs measured with PTR-MS at an urban site of India: Role of emissions, meteorology and photochemical sources. Environ. Pollut. 258,113651.

Mao, J., Ren, X., Chen, S., Brune, W., Chen, Z., Martinez, M., Harder, H., Lefer, B., Rappengluck, B., Flynn, J., Leuchner, M., 2010. Atmospheric oxidation capacity in the summer of Houston 2006: comparison with summer measurements in other metropolitan studies. Atmos. Environ. 44, 4107-4115.

Mo, Z., Shao, M., Lu, S., Niu, H., Zhou, M., Sun, J., 2017. Characterization of non-methane hydrocarbons and their sources in an industrialized coastal city, Yangtze River Delta, China. Sci. Total. Environ. 593-594, 641-653.

Norris, G., Duvall, R., Brown, S., Bai, S., 2014. EPA Positive Matrix Factorization (PMF) 5.0 Fundamentals and User Guide, U.S. Environmental Protection Agency National Exposure Research Laboratory Research Triangle Park, NC.

Prinn, R., 2003. The cleansing capacity of the atmosphere. Annu. Rev. Environ. Resour. 28, 29-57.

Ren, Y., Ma, S., Wang, W., Yu, S., Li, Y., Zhang, R., Yin, S., 2020. Ambient VOCs characteristics, ozone formation potential, and source apportionment of air pollution in spring in Zhengzhou. Environ. Sci (in Chinese). 41, 2577-2585.

Ren, X., Brune, W., Mao, J., Mitchell, M., Lesher, R., Simpas, J., Metcalf, A., Schwab, J., Cai, C., Li, Y., 2006. Behavior of OH and HO_2 in the winter atmosphere in New York City. Atmos. Environ. 40, 252-263.

Sadeghi, B., Pouyaei, A., Choi, Y., Rappenglueck, B., 2022. Influence of seasonal variability on source characteristics of VOCs at Houston industrial area. Atmos. Environ. 277, 1190.

880   Schneidemesser, E., Monks, P., Plass-Duelmer, C., 2010. Global comparison of VOC
881   and CO observations in urban areas. Atmos. Environ. 44, 5053–5064.

882   Song, M., Tan, Q., Feng, M., Qu, Y., Liu, X., An, J., Zhang, Y., 2018. Source
883   apportionment and secondary transformation of atmospheric nonmethane
884   hydrocarbons in Chengdu, southwest China. J. Geophys. Res.Atmos. 123,
885   9741-9763.

886   Song, C., Liu, B., Dai, Q., Li, H., Mao, H., 2019a. Temperature dependence and
887   source apportionment of volatile organic compounds (VOCs) at an urban site on
888   the north China plain. Atmos. Environ. 207, 167-181.

889   Song, M., Liu, X., Zhang, Y., Shao, M., Lu, K., Tan, Q., Feng, M., Qu, Y., 2019b.
890   Sources and abatement mechanisms of VOCs in southern China. Atmos. Environ.
891   201, 28-40.

892   Song, S., Shon, Z., Kang, Y., Kim, K., Han, S., Kang, M., Bang, J., Oh, I., 2019c.
893   Source apportionment of VOCs and their impact on air quality and health in the
894   megacity of Seoul. Environ. Pollut. 247, 763-774.

895   Tan, Z., Lu, K., Jiang, M., Su, R., Wang, H., Lou, S., Fu, Q., Zhai, C., Tan, Q., Yue, D.,
896   Chen, D., Wang, Z., Xie, S., Zeng, L., Zhang, Y., 2019. Daytime atmospheric
897   oxidation capacity in four Chinese megacities during the photochemically
898   polluted season: a case study based on box model simulation, Atmos. Chem.
899   Phys. 19, 3493-3513.

900   Uttamang, P., Campbell, p., Aneja, V., Hanna, A., 2020. A multi-scale model analysis
901   of ozone formation in the Bangkok Metropolitan Region, Thailand. Atmos.
902   Environ. 229,117433.

903   Ulbrich, I., Canagaratna, MR., Zhang, Q., Worsnop, D., Jimenez, J., 2009.
904   Interpretation of organic components from positive matrix factorization of
905   aerosol mass spectrometric data. Atmos. Chem. Phys. 9, 2891–2918.

906   Warneke, C., 2004. Comparison of daytime and nighttime oxidation of biogenic and
907   anthropogenic VOCs along the New england coast in summer during New
908   england air quality study 2002. J. Geophys. Res. 109, D10309.

909   Wang, M., Lu, S., Shao, M., Zeng, L., Zheng, J., Xie, F., Lin, H., Hu, K., Lu, X.,

910   2021a. Impact of COVID-19 lockdown on ambient levels and sources of volatile

911   organic compounds (VOCs) in Nanjing, China. Sci. Total Environ. 757, 143823.

912   Wang, Y., Zhu, S., Ma, J., Shen, J., Wang, P., Wang, P., Zhang, H., 2021b. Enhanced

913   atmospheric oxidation capacity and associated ozone increases during

914   COVID-19 lockdown in the Yangtze River Delta. Sci. Total Environ. 768,

915   144796.

916   Wang, S., Yin, S., Zhang, R., Yang, L., Zhao, Q., Zhang, L., Yan, Q., Jiang, N., Tang,

917   X., 2019. Insight into the formation of secondary inorganic aerosol based on

918   high-time-resolution data during haze episodes and snowfall periods in

919   Zhengzhou, China. Sci. Total Environ. 660, 47-56.

920   Wu, F., Yu, Y., Sun, J., Zhang, J., Wang, J., Tang, G., Wang, Y., 2016. Characteristics,

921   source apportionment and reactivity of ambient volatile organic compounds at

922   Dinghu Mountain in Guangdong Province, China. Sci. Total Environ. 548-549,

923   347-359.

924   Xiong, Y., Du, K., 2020. Source-resolved attribution of ground-level ozone

925   formation potential from VOC emissions in Metropolitan Vancouver, BC. Sci.

926   Total Environ. 721, 137698.

927   Xu, Z., Huang, X., Nie, W., Chi, X., Xu, Z., Zheng, L., Sun, P., Ding, A., 2017.

928   Influence of synoptic condition and holiday effects on VOCs and ozone

929   production in the Yangtze River Delta region, China. Atmos. Environ. 168,

930   112-124.

931   Xue, L., Gu, R., Wang, T., Wang, X., Saunders, S., Blake, D., Louie, P., Luk, C.,

932   Simpson, I., Xu, Z., Wang, Z., Gao, Y., Lee, S., Mellouki, A., Wang, W., 2016.

933   Oxidative capacity and radical chemistry in the polluted atmosphere of Hong

934   Kong and Pearl River Delta region: analysis of a severe photochemical smog

935   episode. Atmos. Chem. Phys. 16, 9891-9903.

936   Yadav, R., Sahu, L., Tripathi, N., Pal, D., Beig, G., Jaaffrey, S., 2019. Investigation of

937   emission characteristics of NMVOCs over urban site of western India. Environ.

938   Pollut. 252, 245-255.

939 Yan, D., Lei, Y., Shi, Y., Zhu, Q., Li, L., Zhang, Z., 2018. Evolution of the
940   spatiotemporal pattern of $PM_{2.5}$ concentrations in China – A case study from the
941   Beijing-Tianjin-Hebei region. Atmos. Environ. 183, 225-233.

942 Yan, Y., Peng, L., Li, R., Li, Y., Li, L., Bai, H., 2017. Concentration, ozone formation
943   potential and source analysis of volatile organic compounds (VOCs) in a thermal
944   power station centralized area: A study in Shuozhou, China. Environ. Pollut.
945   223,295-304.

946 Yang, Y., Shao, M., Keßel, S., Li, Y., Lu, K., Lu, S., Williams, J., Zhang, Y., Zeng, L.,
947   Nölscher, A., Wu, Y., Wang, X., Zheng, J., 2017. How the OH reactivity affects
948   the ozone production efficiency: case studies in Beijing and Heshan, China,
949   Atmos. Chem. Phys. 17, 7127-7142.

950 Yang, Y., Liu, X., Zheng, J., Tan, Q., Feng, M., Qu, Y., An, J., Cheng, N., 2019.
951   Characteristics of one-year observation of VOCs, NOx, and O_3 at an urban site in
952   Wuhan, China. J. Environ. Sci. (in China). 79, 297-310.

953 Yang, Y., Wang, Y., Yao, D., Zhao, S., Yang, S., Ji, D., Sun, J., Wang, Y., Liu, Z., Hu,
954   B., Zhang, R., Wang, Y., 2020a. Significant decreases in the volatile organic
955   compound concentration, atmospheric oxidation capacity and photochemical
956   reactivity during the National Day holiday over a suburban site in the North
957   China Plain. Environ. Pollut. 263, 114657.

958 Yang, Y., Wang, Y., Zhou, P., Yao, D., Ji, D., Sun, J., Wang, Y., Zhao, S., Huang, W.,
959   Yang, S., Chen, D., Gao, W., Liu, Z., Hu, B., Zhang, R., Zeng, L., Ge, M., Petäjä,
960   T., Kerminen, V., Kulmala, M., Wang, Y., 2020b. Atmospheric reactivity and
961   oxidation capacity during summer at a suburban site between Beijing and Tianjin.
962   Atmos. Chem. Phys. 20, 8181-8200.

963 Yang, Y., Wang, Y., Huang, W., Yao, D., Zhao, S., Wang, Y., Wang, Y., Ji, D., Zhang,
964   R., Wang, Y., 2021. Parameterized atmospheric oxidation capacity and speciated
965   OH reactivity over a suburban site in the North China Plain: A comparative study
966   between summer and winter. Sci. Total Environ.773, 145264.

967 Yao, D., Tang, G., Wang, Y., Yang, Y., Wang, L., Chen, T., He, H., Wang, Y., 2021.

968   Significant contribution of spring northwest transport to volatile organic

969   compounds in Beijing. J. Environ. Sci. (in China). 104, 169-181.

970 Yuan, B., Shao, M., de Gouw, J., Parrish, D., Lu, S., Wang, M., Zeng, L., Zhang, Q.,

971   Song, Y., Zhang, J., Hu, M., 2012. Volatile organic compounds (VOCs) in urban

972   air: how chemistry affects the interpretation of positive matrix factorization

973   (PMF) analysis. J. Geophys. Res.-Atmos. 117, D24302.

974 Zhang, F., Shang, X., Chen, H., Xie, G., Fu, Y., Wu, D., Sun, W., Liu, P., Zhang, C.,

975   Mu, Y., Zeng, L., Wan, M., Wang, Y., Xiao, H., Wang, G., Chen, J., 2020.

976   Significant impact of coal combustion on VOCs emissions in winter in a North

977   China rural site. Sci. Total Environ. 720, 137617.

978 Zhang, G., Xu, H., Qi, B., Du, R., Gui, K., Wang, H., Jiang, W., Liang, L., Xu, W.,

979   2018. Characterization of atmospheric trace gases and particulate matter in

980   Hangzhou, China. Atmos. Chem. Phys. 18, 1705-1728.

981 Zhang, X., Yin, Y., Wen, J., Huang, S., Han, D., Chen, X., Cheng, J., 2019.

982   Characteristics, reactivity and source apportionment of ambient volatile organic

983   compounds (VOCs) in a typical tourist city. Atmos. Environ. 215, 116898.

984 Zhang, Y., Wang, X., Zhang, Z., Lu, S., Huang, Z., Li, L., 2015. Sources of C(2)-C(4)

985   alkenes, the most important ozone nonmethane hydrocarbon precursors in the

986   Pearl River Delta region. Sci. Total Environ. 502, 236-245.

987 Zheng, H., Kong, S., Xing, X., Mao, Y., Hu, T., Ding, Y., Li, G., Liu, D., Li, S., Qi, S.,

988   2018. Monitoring of volatile organic compounds (VOCs) from an oil and gas

989   station in northwest China for 1 year. Atmos. Chem. Phys. 18, 4567-4595.

990 Zheng, H., Kong, S., Yan, Y., Chen, N., Yao, L., Liu, X., Wu, F., Cheng, Y., Niu, Z.,

991   Zheng, S., Zeng, X., Yan, Q., Wu, J., Zheng, M., Liu, D., Zhao, D., Qi, S., 2020.

992   Compositions, sources and health risks of ambient volatile organic compounds

993   (VOCs) at a petrochemical industrial park along the Yangtze River. Sci. Total

994   Environ. 703, 135505.

995 Zheng, H., Kong, S., Chen, N., Niu, Z., Zhang, Y., Jiang, S., Yan, Y., Qi, S., 2021.

996   Source apportionment of volatile organic compounds: Implications to reactivity,

997   ozone formation, and secondary organic aerosol potential. Atmos. Res. 249,

105344.

Zhou, X., Li, Z., Zhang, T., Wang, F., Wang, F., Tao, Y., Zhang, X., Wang, F., Huang, J., 2019. Volatile organic compounds in a typical petrochemical industrialized valley city of northwest China based on high-resolution PTR-MS measurements: Characterization, sources and chemical effects. Sci. Total Environ. 671, 883-896.

Zhu, J., Wang, S., Wang, H., Jing, S., Lou, S., Saiz-Lopez,A., Zhou, B., 2020. Observationally constrained modeling of atmospheric oxidation capacity and photochemical reactivity in Shanghai, China. Atmos. Chem. Phys. 20, 1217-1232.

Zou, Y., Deng, X., Zhu, D., Gong, D., Wang, H., Li, F., Tan, H., Deng, T., Mai, B., Liu, X., Wang, B., 2015. Characteristics of 1 year of observational data of VOCs, NOx and O_3 at a suburban site in Guangzhou, China. Atmos. Chem. Phys. 15, 6625-6636.

Figure list:

Fig. 1 Locations of the sampling stations in Zhengzhou.
.
Fig. 2 Monthly changes in the concentrations of VOCs in Zhengzhou. The upper and lower boundaries of the boxes indicate the 75th and 25th percentiles, respectively; the lines within the boxes mark the median; the whiskers above and below the boxes indicate the 90th and 10th percentiles, respectively.

Fig. 3 Diurnal variations in VOCs compounds measured at Zhengzhou. The upper and lower boundaries of the boxes indicate the 75th and 25th percentiles, respectively; the lines within the boxes mark the median; the whiskers above and below the boxes indicate the 90th and 10th percentiles, respectively.

Fig. 4 Source profiles and contribution percentages from each source during the observation period by PMF model (bar is a mixing ratio and dot is a percentage).

Fig. 5 Directional dependence and hourly record of each source in Zhengzhou.

Fig. 6 The contributions of each VOC source during 2018-2020.

Fig. 7 Seasonal variation of source contributions to VOCs concentration.

Fig. 8 Comparison of the relative contributions of OH, O_3 and NO_3 of the AOC in Zhengzhou during the sampling periods.

Fig. 9 Comparison of the relative contributions the OH reactivity in Zhengzhou .

Fig. 10 Top 10 VOCs species that contributed most to the Propy-Equiv and MIR weighted concentrations in Zhengzhou.
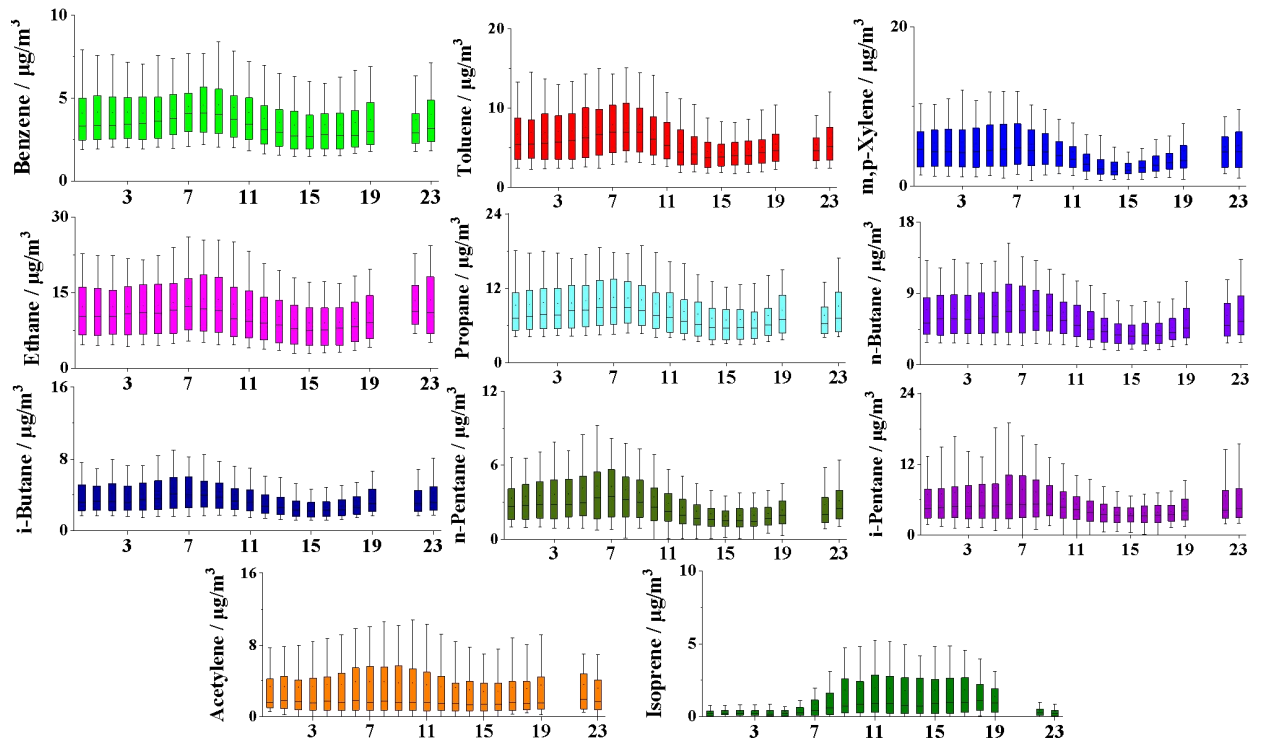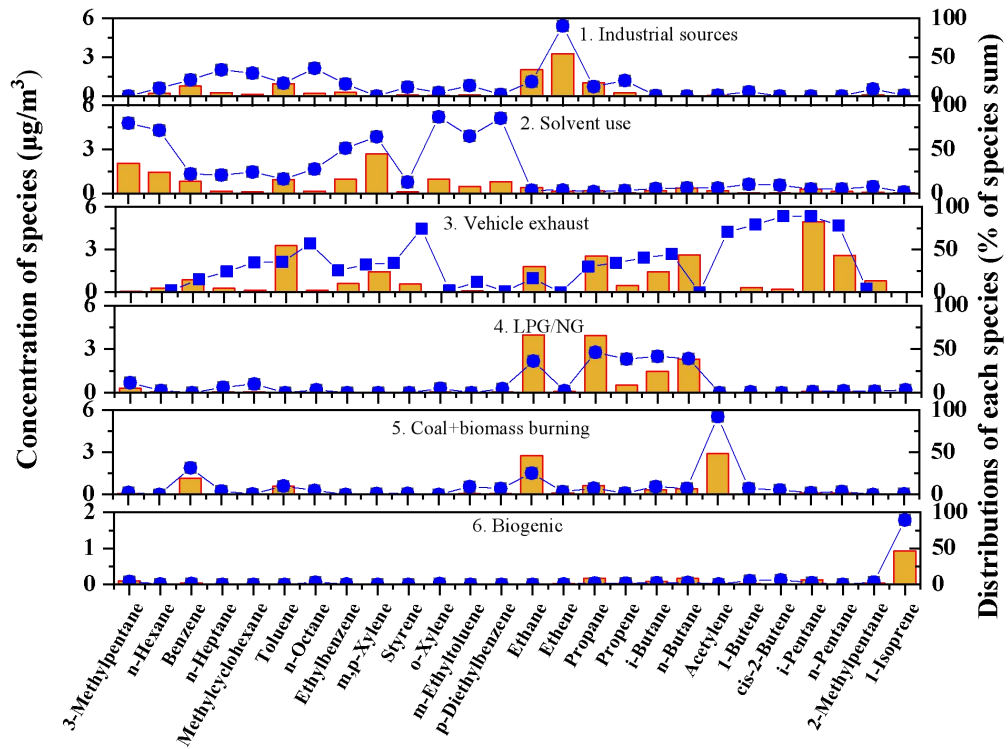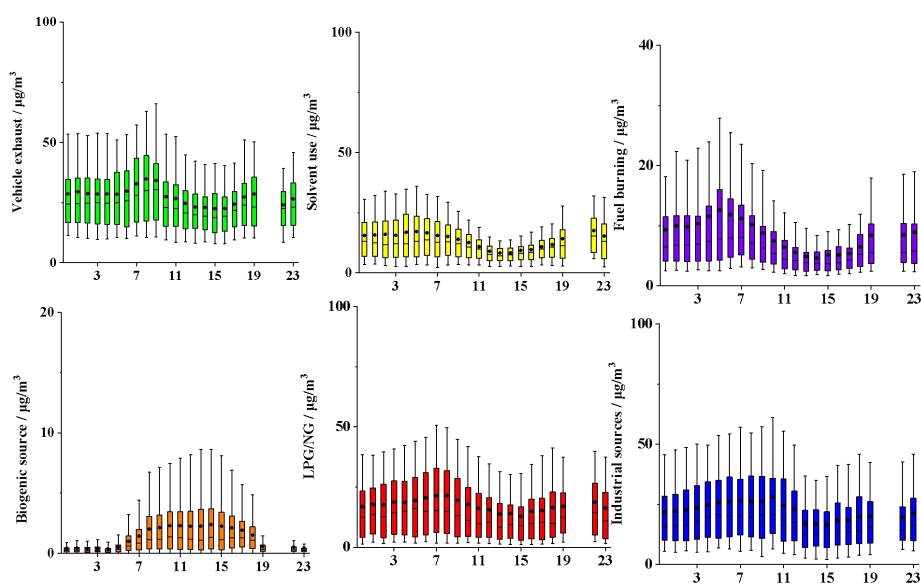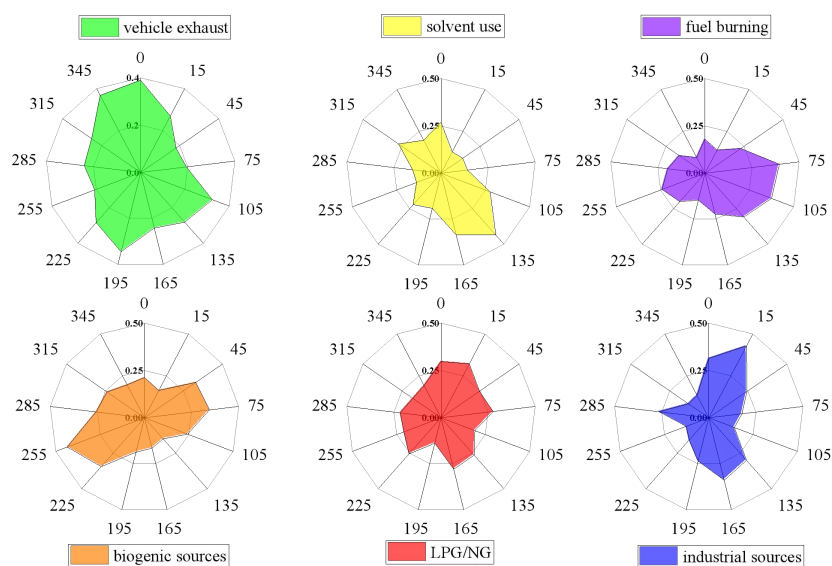
1043

1044

1045 **Fig. 1** Locations of the sampling stations, and Fig. a-c represents China, Henan and
1046 Zhengzhou respectively.

1047

Fig. 2 Monthly changes in the concentrations of the typical VOCs species in Zhengzhou. The upper and lower boundaries of the boxes indicate the 75th and 25th percentiles, respectively; the lines within the boxes mark the median; the whiskers above and below the boxes indicate the 90th and 10th percentiles, respectively.

1057

1058

1059 **Fig. 3** Diurnal variations in VOCs compounds measured at Zhengzhou. The upper and
1060 lower boundaries of the boxes indicate the 75th and 25th percentiles, respectively; the
1061 lines within the boxes mark the median; the whiskers above and below the boxes
1062 indicate the 90th and 10th percentiles, respectively.

1063

Fig.4 Source profiles and contribution percentages during the observation period by PMF model (bar is a mixing ratio and dot is a percentage).

1068

1069
1070
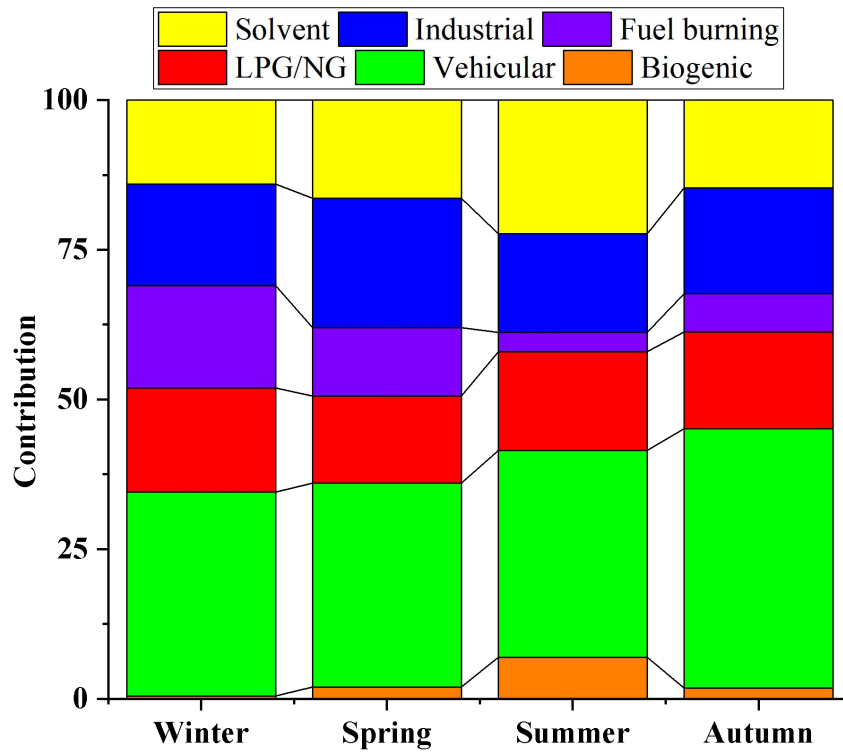1071 **Fig. 5** Directional dependence and hourly record of each source in Zhengzhou.
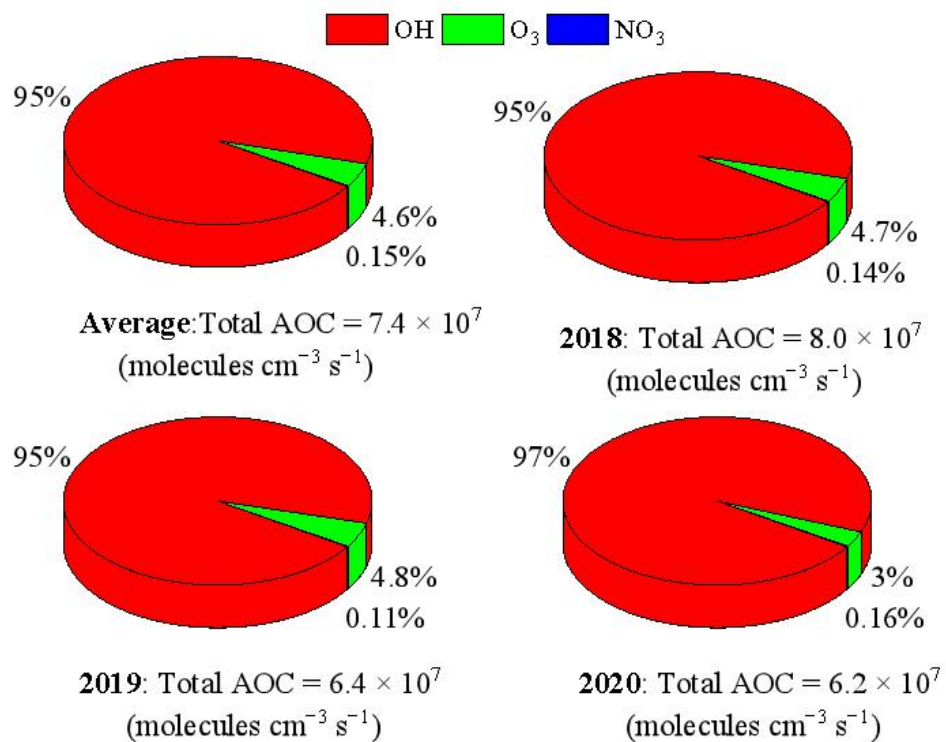1072

1073
1074

Fig. 6 The contributions of each VOC source during 2018-2020.

1075

1076

1077

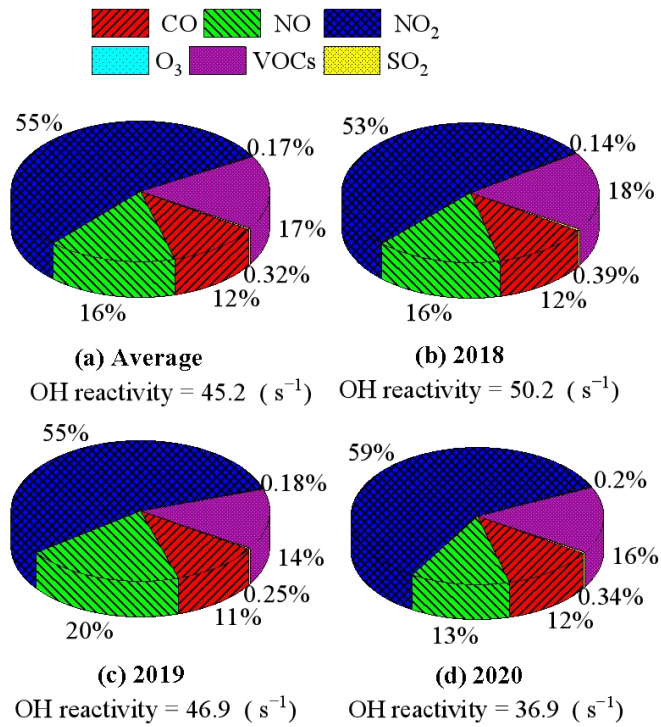**Fig. 7** Seasonal variation of source contributions to VOCs concentration.

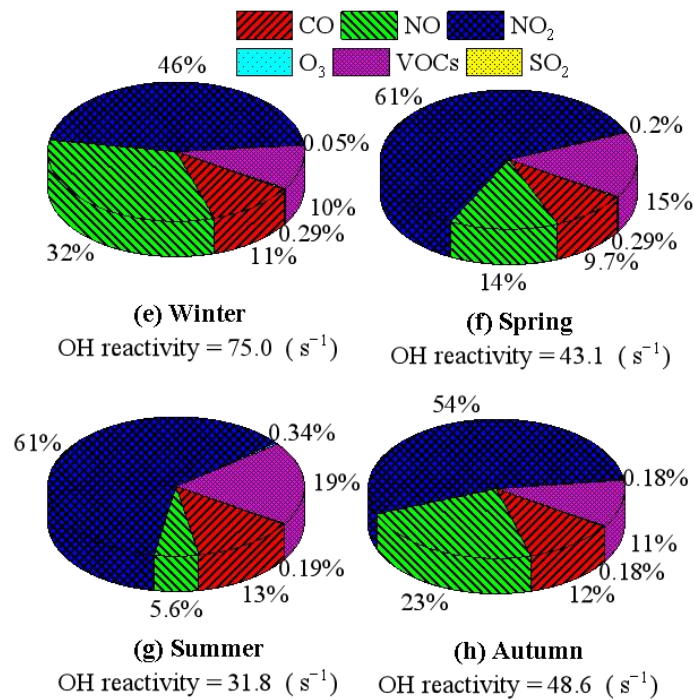**Fig. 8** Comparison of the relative contributions of OH, O_3 and NO_3 of the AOC in Zhengzhou during the sampling periods.

1087

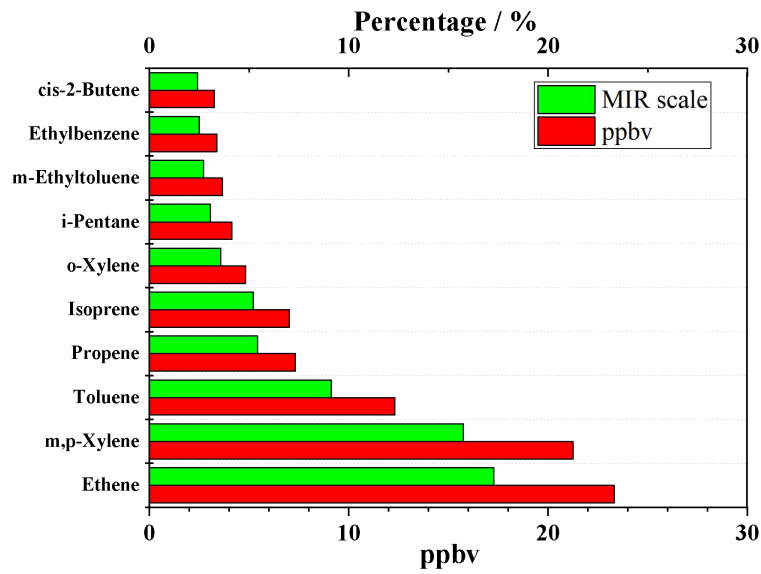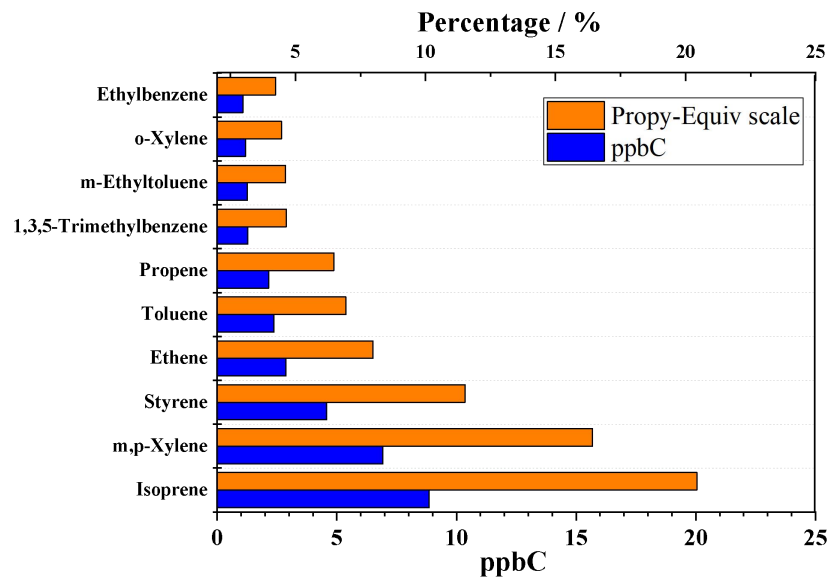**Fig. 9** Comparison of the relative contributions the OH reactivity in Zhengzhou .

1093
1094

1095

1096
1097 **Fig. 10** Top 10 VOCs species that contributed most to the Propy-Equiv and MIR
1098 weighted concentrations in Zhengzhou.
1099

Table list:

Table 1 Top 20 most abundant VOC species (μg/m^3) measured in Zhengzhou for the study period 2018-2020.

Table 2 Comparison of source contributions resolved by PMF models in different cities.

Table 1 Top 20 most abundant VOC species (μg/m^3) measured in Zhengzhou for the
study period 2018-2020.

Species	2018	Species	2019	Species	2020	Species	Average
Ethane	13.4±7.5	Ethane	11.6±7.7	Ethane	10.2±5.3	Ethane	11.7±6.8
Propane	8.6±5.2	Propane	8.8±5.6	Propane	7.3±4	Propane	8.2±4.9
i-Pentane	7.9±19.7	n-Butane	6.2±4.7	Toluene	5.6±4.3	Toluene	6.5±4.5
Toluene	7.8±4.3	Toluene	6.1±4.7	Ethene	5.5±4.4	i-Pentane	6.1±10.4
Ethene	7.6±6.2	i-Pentane	6±6.8	n-Butane	5.4±3.7	n-Butane	5.8±4.1
n-Pentane	6±16.1	m,p-Xylene	4.5±4.4	i-Pentane	4.6±4.7	Ethene	5.6±5.3
n-Butane	5.9±3.8	Benzene	3.9±2.4	m p-Xylene	4.3±5.4	m p-Xylene	4.7±4.3
m--p-Xylene	5.2±3	Ethene	3.8±5.3	i-Butane	3.5±2.2	Benzene	3.8±2.3
Acetylene	4.9±5	i-Butane	3.8±2.7	Benzene	3.4±1.9	n-Pentane	3.8±7.3
Cyclopentane	4.4±23.4	n-Hexane	3.7±3.5	n-Pentane	2.3±2.8	i-Butane	3.5±2.4
Benzene	4.1±2.5	Acetylene	3.3±4.8	Ethylbenzene	2±2	Acetylene	3±3.6
i-Butane	3.1±2.1	n-Pentane	3.1±2.9	Isoprene	1.9±3.4	Ethylbenzene	2.4±1.8
Ethylbenzene	3.1±1.8	3-Methylpentane	2.6±1.9	n-Hexane	1.1±1.3	n-Hexane	2.2±2.2
Isoprene	2.8±3.2	Ethylbenzene	2.1±1.6	Styrene	1.1±1.7	Cyclopentane	2±9
n-Hexane	1.9±1.6	Propene	1.6±1.9	o-Xylene	1.1±1.4	1-Isoprene	1.9±2.8
o-Xylene	1.7±1	o-Xylene	1.2±1.1	Propene	1±2.2	3-Methylpentane	1.7±1.5
3-Methylpentane	1.7±1.6	2-Methylpentane	1.1±1.4	n-Heptane	1±1.6	o-Xylene	1.4±1.2
Styrene	1.6±1.2	Isoprene	1.1±1.9	m-Ethyltoluene	1±1.2	Propene	1.3±1.7
p-Diethylbenzene	1.6±1.2	Cyclopentane	1.1±2.2	n-Undecane	1±1.7	Styrene	1.2±1.3
Propene	1.4±0.9	p-Diethylbenzene	1±0.9	n-Dodecane	1±2.4	p-Diethylbenzene	1.2±1
∑TOP 20 species/∑VOCs	84%		84%		81%		83%

1115 **Table 2** Comparison of source contributions resolved by PMF models in different
1116 cities (%).

City	Sampling periods	Solvent use	Industrial sources	Vehicle exhaust	Fuel burning	LPG/ NG	Biogenic sources
Taiwan[a]	January–December 2016	29	15	18	-	-	4
Wuhan[b]	September 1, 2016 to August 31, 2017		16	24	19	13	2
Shuozhou[c]	March and August, 2014	-	14	21	30	18	-
Ningbo[d]	December 2012, April 2013, July 2013, and October 2013	7	50	16	-	27	-
Beijing[e]	March 2016 to January 2017	16	10	19	-	12	8
This study	January 2018 to December 2020	17	18	36	10	16	3

1117 (a:Huang et al., 2019; b:Hui et al., 2018; c: Yan et al., 2017; d: Mo et al., 2017; e: Li et al., 2020c.)

1118

1119